

# EFFECT OF NITROGEN ON THE THERMAL DEFORMATION BEHAVIOR OF MARTENSITIC STAINLESS BEARING STEEL

## VPLIV DUŠIKA NA TOPLOTNO DEFORMACIJO MARTENZITNEGA NERJAVNEGA LEŽAJNEGA JEKLA

Yaohui Song<sup>1</sup>, Yibo Lu<sup>2</sup>, Yugui Li<sup>2\*</sup>, Haosong Sun<sup>3</sup>, Huaying Li<sup>3</sup>, Hui Xu<sup>3</sup>,  
Yihang Wang<sup>2</sup>

<sup>1</sup>Heavy Machinery Education Engineering Department Research Center, Taiyuan University of Science and Technology, Taiyuan, 030024, Shanxi, China

<sup>2</sup>School of Mechanical Engineering, Taiyuan University of Science and Technology, Taiyuan 030024, Shanxi, China

<sup>3</sup>School of Materials Science and Engineering, Taiyuan University of Science and Technology, Taiyuan 030024, Shanxi, China

*Prejem rokopisa – received: 2024-05-16; sprejem za objavo – accepted for publication: 2024-10-24*

doi:10.17222/mit.2024.1194

The thermal deformation behaviors of martensitic stainless bearing steels (0.16N, 0N) in the temperature range 850–1150 °C, strain rate 0.01–10 s<sup>-1</sup>, and deformation of 60 % were studied using a single-pass compression experiment. After adding 0.16 % nitrogen, the peak stress of the martensitic stainless bearing steel increased under all thermal forming conditions, and the average peak stress increased by about 33.724 MPa. The strain-rate sensitivity diagram, power dissipation diagram, instability factor diagram, and thermal processing diagram under different strains were constructed based on the stress-strain curve. The thermal deformation activation energy under different strains was constructed and combined with a metallographic structure analysis. The results show that under the same conditions, the occurrence of DRX in 0.16N bearing steel is less than that of 0N bearing steel, but the grains are finer than those of 0N bearing steel.

Keywords: martensitic stainless bearing steel, thermal deformation behavior, power dissipation diagram, thermal deformation activation energy, thermal processing diagram

Avtorji v članku opisujejo študijo obnašanja dveh martenzitivnih ležajnih jekel; enega brez dušika in drugega legiranega z 0,16 w/% N (označenih kot 0N in 0.16N), med toplotno (termično) tlačno deformacijo v temperaturnem območju med 850 °C in 1150 °C, pri hitrosti deformacije med 0,01 s<sup>-1</sup> in 10 s<sup>-1</sup> ter 60 % deformacijo. Po legiranju jekla z 0,16 w/% dušika se je maksimalna tlačna napetost martenzitivnega nerjavnega ležajnega jekla znatno povečala pri vseh izbranih pogojih termične deformacije. V povprečju je ta napetost znašala približno 33,724 MPa. Avtorji so na osnovi izvedenih eksperimentov in dobljenih diagramov *napetost-deformacija* konstruirali diagram občutljivosti na hitrost deformacije, disipacijski diagram moči, diagram faktorja nestabilnosti in diagram termičnega procesiranja. Avtorji so konstruirali tudi diagrame termične aktivacijske energije za deformacijo pri različnih deformacijah in ga kombinirali z metalografskimi analizami mikrostrukture. Rezultati analiz so nadalje pokazali, da je pri enakih pogojih termične deformacije obseg dinamične rekristalizacije (DRX) pri ležajnem jeklu 0.16N manjši kot pri ležajnem jeklu 0N, toda z dušikom legirano jeklo ima finejša kristalna zrna.

Ključne besede: martenzitivno nerjavno ležajno jeklo, termična deformacija, diagram raztrosa moči, aktivacijska energija toplotne deformacije, diagram toplotnega procesiranja

## 1 INTRODUCTION

Bearings are essential components in modern industrial systems, affecting the stability and longevity of mechanical equipment. Selecting the right bearing steel is critical, as high-quality materials provide superior mechanical properties, including strength, hardness, and resistance to wear and shock.<sup>1</sup> However, traditional, high-carbon, chromium martensitic stainless steels, such as 9Cr18 and 9Cr18Mo, are limited by the presence of coarse eutectic carbides.<sup>2</sup> Nitrogen alloying has been shown to refine carbides and grains, enhancing the steel's strength without sacrificing toughness, making nitrogen-containing martensitic stainless steel a promising candidate for high-performance bearings.<sup>3</sup> Research has predominantly focused on optimizing thermal treatment processes and improving the material's corrosion, fa-

tigue, and impact resistance.<sup>4</sup> For effective production of nitrogen-alloyed bearing forgings, it is crucial to explore the material's plastic deformation behavior, microstructural evolution, and thermal processing properties at elevated temperatures. This study aims to establish a solid theoretical basis and practical guidelines for optimizing the thermal forging parameters, ensuring that stainless-steel bearings achieve the desired microstructure and mechanical properties during manufacture.<sup>5-8</sup>

In recent years, researchers have made the following studies on stainless bearing steel. Zhang et al.<sup>9</sup> studied the effects of forming temperature and strain rate on the austenitizing and dynamic recrystallization of 30CrMnSiNi2A steel. According to the experimental results, the constitutive equation and machining diagram of 30CrMnSiNi2A steel are established. The unsafe zone of 30CrMnSiNi2A steel is not only distributed in the region with low temperature and low strain rate but also in the

\*Corresponding author's e-mail:  
lygtykd@163.com (Yugui Li)

region with high temperature and high strain rate. 30CrMnSiNi2A steel exhibits ideal thermoplastic formability when heat treated at 1050 °C at a strain rate of 0.1–1 s<sup>-1</sup>. Feng et al.<sup>10</sup> developed a machining diagram of a 20CrMnTiH steel using a dynamic material model in the temperature range 850–1150 °C and a strain variability of 0.01–1 s<sup>-1</sup>. According to the developed machining diagram, the thermal working characteristics of 20CrMnTiH steel are analyzed, and the optimal thermal working parameter values of 20CrMnTiH steel are found to obtain good thermal working properties and a small grain size in the process parameter range of 1036–1070 °C, 0.1–1 s<sup>-1</sup>. Lin et al.<sup>11</sup> studied the dynamic recrystallization mechanism of bearing steel G13Cr4Mo4Ni4V. The results show that because the deformation ability of ferrite and carbide is different from that of the matrix, their dissolution, precipitation behavior, and interaction with dislocation during deformation are the main reasons for inducing steel recrystallization.

Despite numerous studies on the properties of martensitic stainless steel, research focusing on the influence of nitrogen content on its thermal deformation behavior under high-temperature conditions is relatively scarce, limiting the material’s further development and application. To address this gap, we systematically investigated two types of bearing steels: nitrogen-containing martensitic stainless bearing steel (0.16N) and nitrogen-free martensitic stainless bearing steel (0N). Through single-pass compression experiments conducted at temperatures ranging from 850 °C to 1150 °C, strain rates of 0.01 s<sup>-1</sup> to 10 s<sup>-1</sup>, and 60 % deformation, we established comprehensive thermal processing maps based

on stress-strain curves. These maps include strain-rate sensitivity diagrams, power-dissipation diagrams, instability-factor diagrams, and thermal processing diagrams under different strains, providing a new theoretical foundation for optimizing hot-working processes. Additionally, we calculated the thermal deformation activation energy and combined it with metallographic structure analyses to reveal the mechanisms by which nitrogen addition influences dynamic recrystallization and grain refinement. This study seeks to contribute to the understanding of how nitrogen affects the thermal deformation behavior of martensitic stainless bearing steel, offering insights that might assist in enhancing its performance through controlled hot-working practices.

## 2 EXPERIMENTAL PART

The alloys used in this study are bearing steel with a nitrogen content of 0.16 % (from now on referred to as 0.16N) and nitrogen-free bearing steel (from now on referred to as 0N), both of which are cut in to incompletely forged ingots with a forging ratio of 1:2. The primary chemical constituents are shown in **Table 1**. The cylindrical compression specimens of 0.16N and 0N were prepared, with a height of 15 mm and a diameter of 10 mm. A Gleeble-3800 thermal simulation testing machine conducted the thermal compression test in a vacuum. In order to reduce the influence of friction and prevent adhesion between the sample and the equipment, graphite lubricant was coated on both ends of the sample, and a tantalum sheet and graphite sheet were added.

The thermal compression process is shown in **Figure 1a**. The test strain rates are 0.01–10 s<sup>-1</sup>, respectively;

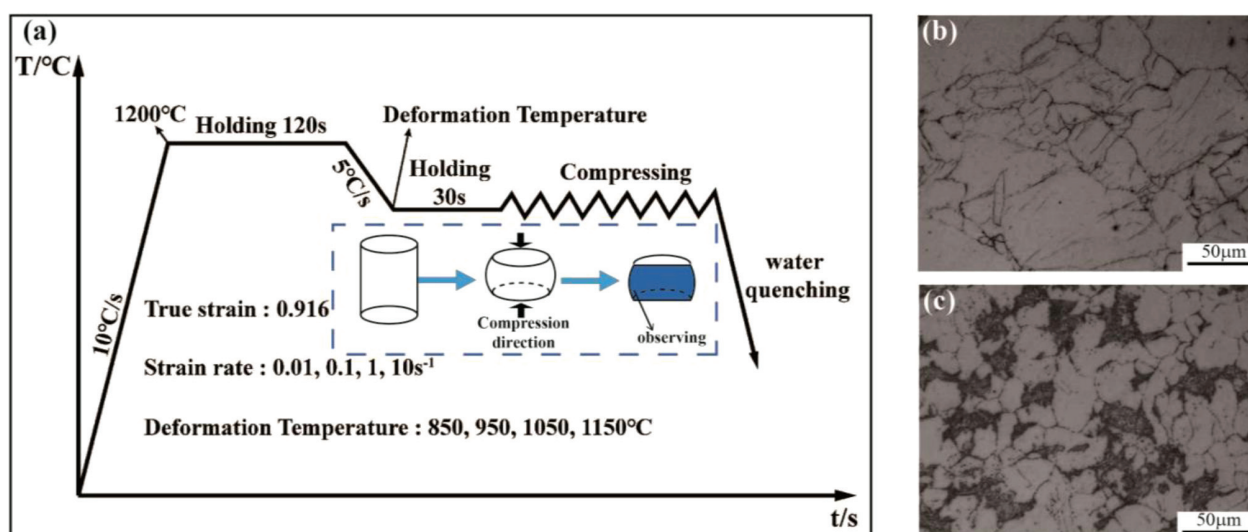


**Figure 1:** a) Schematic of the thermal deformation process; Original microstructure: b) 0.16N, c) 0N

**Table 1:** Chemical composition of 0.16N and 0N (w%)

Materials	C	Si	Mn	P	Cr	Mo	N	Fe
0.16N	0.3	0.51	0.42	0.002	15.16	0.83	0.16	Bal.
0N	0.3	0.51	0.42	0.002	15.16	0.83	0.00	Bal.

the temperature range is 850–1150 °C, the deformation rate is 60 %, and the true strain is 0.916. The specific process is heating at 10 °C/s to 1200 °C for 2 min and then cooling at 5 °C/s to the deformation temperature, compression after 30 s, and water cooling immediately after compression to retain the high-temperature tissue. The compressed sample was cut along the compression direction and heated in a water bath with 2g  $\text{KMnO}_4$  + 6 mL  $\text{H}_2\text{SO}_4$  + 94 mL  $\text{H}_2\text{O}$  etchant for 40 min. Then, OM was used to observe the metallographic structure. The original microstructure is shown in **Figures 1b** and **1c**.

### 3 RESULTS

#### 3.1 Stress-strain curve

The stress-strain curves obtained by thermal compression of 0.16N and 0N stainless bearing steels are shown in **Figure 2**. The trend of experimental curves of the two kinds of steel is generally the same, and the flow stress of the material increases with the increase of strain rate under the condition of keeping the deformation temperature unchanged. Under the same strain-rate condi-

tion, the flow stress of the material shows a decreasing trend with an increase in temperature. This indicates that both steels are positively sensitive to strain rate and negatively sensitive to temperature. In addition, under the same conditions, the flow stress of 0.16N bearing steel is higher than that of 0N bearing steel. It can be seen from **Figure 2i** that after adding 0.16 % nitrogen, the peak stress under all thermal forming conditions is increased, and about 33.724 MPa increases the average peak stress. This data indicates that the addition of nitrogen has a positive effect on improving the deformation resistance of the material. Especially when the deformation is carried out at 850 °C and the low strain rate of 0.1  $\text{s}^{-1}$ , the increase in the stress value is particularly prominent, which indicates that the solid solution strengthening of nitrogen and the nailing effect of carbides and nitrides are the most significant under this condition. The consistent trend in the overall increment ratio shown in **Figure 2i** indicates that the increase in deformation resistance is uniform and steady, which helps to ensure that the material maintains high-performance stability over a wide range of application conditions.

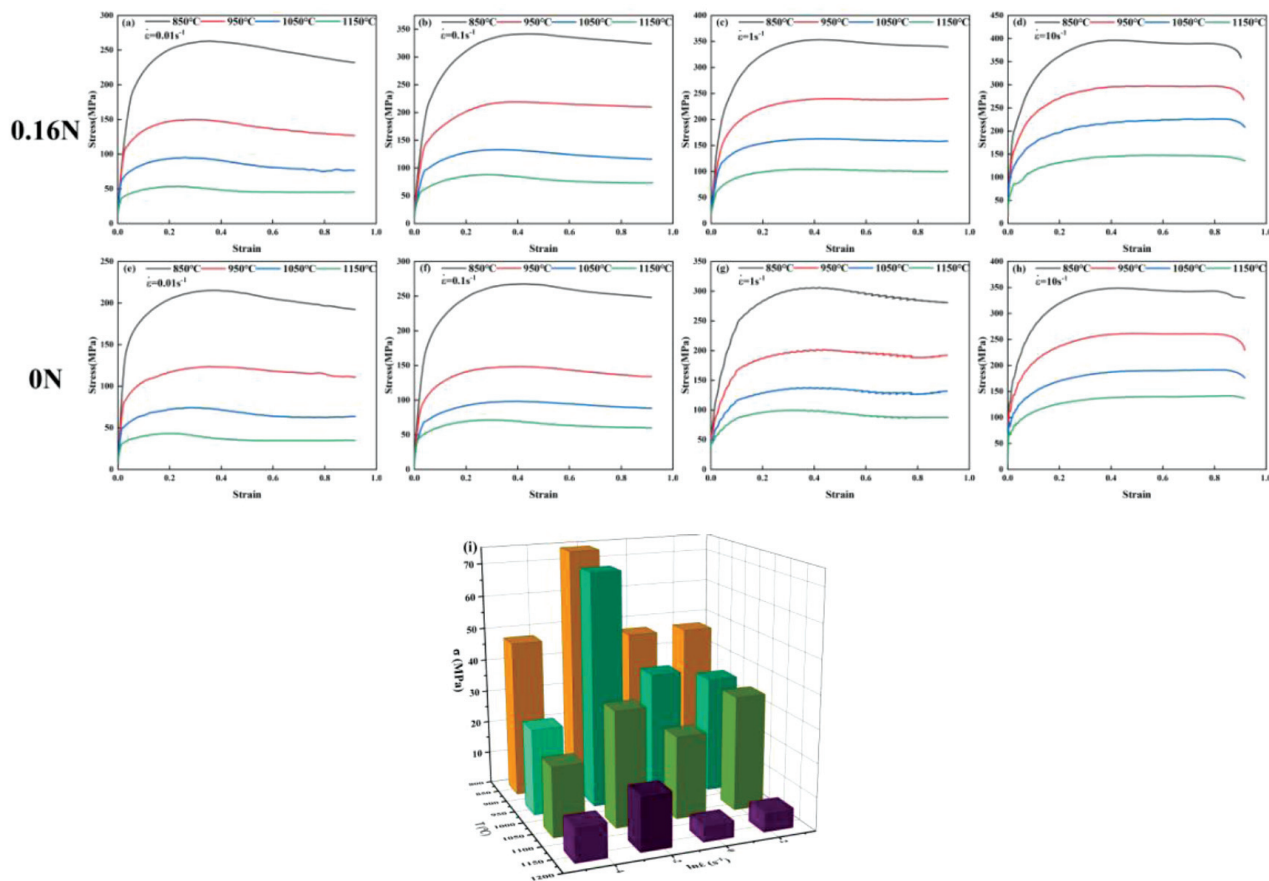


**Figure 2:** Stress-strain curves of 0.16N at different rates: a) 0.01s<sup>-1</sup>, b) 0.1 s<sup>-1</sup>, c) 1 s<sup>-1</sup>, d) 10 s<sup>-1</sup>; stress-strain curves of 0N at different rates: e) 0.01 s<sup>-1</sup>, f) 0.1 s<sup>-1</sup>, g) 1 s<sup>-1</sup>, h) 10 s<sup>-1</sup>; i) comparison diagram of peak-stress difference and increment between 0.16N and 0N

### 3.2 Comparison of thermal processing properties

#### 3.2.1 Strain-rate sensitivity index

Generally speaking, the strain rate affects the high-temperature deformation characteristics of steel. In order to understand the effect of strain rate on material behavior deeply, many researchers have introduced the strain-rate sensitivity index to conduct in-depth studies of various materials. The specific mathematical expression of the index is as follows:<sup>12</sup>

$$m = \frac{\partial(\ln \sigma)}{\partial(\ln \dot{\sigma})} \quad (1)$$

**Figure 3** shows the strain-rate sensitivity diagram of 0.16N and 0N martensitic stainless bearing steel at strains of 0.3, 0.6, and 0.9. In the process of thermal deformation,  $m$  represents the sensitivity of the flow stress to the strain rate, and the greater  $m$  is, the more sensitive the flow stress of the material is to the strain rate. According to the value of  $m$ , it can be divided into three grades:<sup>13</sup> low  $m$  value ( $m < 0.15$ ), high  $m$  value ( $0.2 < m < 0.3$ ), and superplastic region ( $m > 0.3$ ). By observing the strain-rate sensitivity graphs of the two materials under each strain, we see that the low  $m$ -value region decreases gradually. In contrast, the high  $m$ -value and superplastic regions increase first and then decrease. Taking 0N bearing steel as an example, when the strain is 0.3, the low  $m$  value zone is 950–1075 °C and (1075–1200 °C, 0.13–10 s<sup>-1</sup>); when the strain is increased to 0.7, the main low  $m$  value zone is 950–1000 °C, 0.01–0.05 s<sup>-1</sup> and 950–1000 °C, 2.71–10 s<sup>-1</sup>). When the strain is 0.3, the high  $m$ -value region is located at 1100–1150 °C, 0.01–0.05 s<sup>-1</sup>. With the increase of the strain, the high  $m$  value region first increases and is located at 1025–1150 °C, 0.01–0.08 s<sup>-1</sup> and 1100–1150 °C, 2.71–10 s<sup>-1</sup>. After the area is reduced, located at 1100–1150 °C, 0.01–0.08 s<sup>-1</sup>. The superplastic region of the two materials is slightly different. The superplastic region of the 0N bearing steel is mainly concentrated in 1125–1150 °C,  $\dot{\epsilon} < 4$  s<sup>-1</sup> (under

different strains), while the superplastic region of the 0.16N bearing steel is first concentrated in 1100–1150 °C,  $\dot{\epsilon} < 0.02$  s<sup>-1</sup>. Then, with the increase of strain, the superplastic region of the two materials becomes slightly different. It was gradually transferred to the low-temperature and low-rate region 875–975 °C,  $\dot{\epsilon} < 0.02$  s<sup>-1</sup>. Note that the superplastic phenomenon of 0N bearing steel usually occurs at high temperature and low speed, while the superplastic phenomenon of 0.16N bearing steel tends to shift to low temperature and high speed with increased strain. In addition, it is not difficult to see from the figure that the area of high  $m$  region and superplastic region of 0.16N bearing steel under different strains is larger than that of 0N bearing steel, indicating that the flow stress of 0.16N bearing steel is more sensitive to the strain rate.

#### 3.2.2 Power dissipation efficiency

In thermal processing engineering, different power-dissipation efficiency ( $\eta$ ) values correspond to different microstructure-evolution mechanisms, and the three-dimensional contours consisting of power-dissipation value, temperature, and strain rate are called power-dissipation diagrams. The higher the  $\eta$  value, the better the thermal processability of the region in which it is located, indicating the better microstructure evolution mechanism, while the negative value indicates the possible unstable microstructure.

When the  $m$  value is constant and non-linear with temperature or strain rate, the power-dissipation efficiency ( $\eta$ ) can be expressed as:<sup>14</sup>

$$h = \frac{J}{J_{\max}} = \frac{2m}{m+1} \quad (2)$$

**Figure 4** shows the power-dissipation efficiency of 0.16N and 0N martensitic stainless bearing steel when the strain is 0.3, 0.6, and 0.9. It is not difficult to see that the change in power-dissipation efficiency is very similar to that of the strain-rate sensitivity coefficient: regions

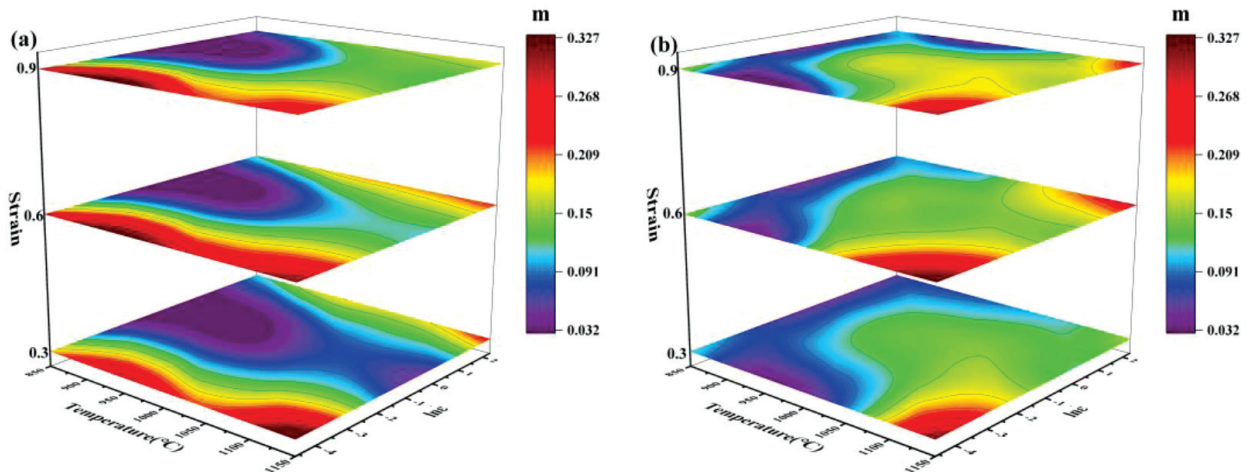


**Figure 3:** Comparison of strain-rate sensitivity index: a) 0.16N bearing steel, b) 0N bearing steel

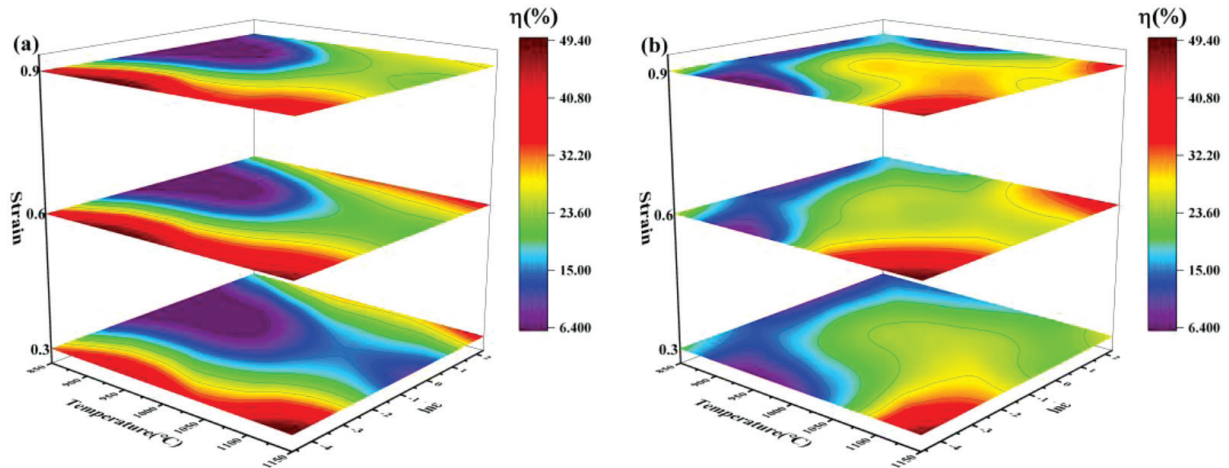


Figure 4: Comparison of power-dissipation values: a) 0.16N bearing steel, b) 0N bearing steel

with low  $\eta$  value ( $\eta < 15\%$ ) gradually decrease, while regions with high  $m$  value increase first and then decrease. The three dynamic evolution processes of work hardening, DRV, and DRX are closely related to the power-dissipation values, and the  $\eta$  value represents different microscopic transformations.  $\eta$  generally reflects the microstructure-deformation mechanism;<sup>13</sup>  $0.2 < \eta < 0.3$  is DRV, and  $0.2 < \eta < 0.3$  is DRX. Taking 0.9 strain as an example, the high  $\eta$  value ( $\eta > 35\%$ ) of 0N bearing steel is mainly concentrated in the high-temperature and low-strain-rate zone ( $1100\text{--}1150\text{ }^\circ\text{C}$ ,  $\dot{\epsilon} < 0.05\text{ s}^{-1}$ ), and the high-temperature and high-strain-rate zone ( $1125\text{--}1150\text{ }^\circ\text{C}$ ,  $\dot{\epsilon} > 4.5\text{ s}^{-1}$ ). The high  $\eta$  value ( $\eta > 35\%$ ) of 0.16N bearing steel is mainly concentrated in the low-strain-rate zone ( $850\text{--}1150\text{ }^\circ\text{C}$ ,  $\dot{\epsilon} < 0.05\text{ s}^{-1}$ ). In the evolution process,  $\eta$  varies from 6.4% to 49.4%. Both steel sheets' high  $\eta$  region occurs at high temperatures and low rates ( $1100\text{--}1150\text{ }^\circ\text{C}$ ,  $\dot{\epsilon} < 0.05\text{ s}^{-1}$ ) because a higher deformation temperature is conducive to grain-boundary migration. In contrast, a lower strain rate provides a longer deformation time and increases the

time for recrystallization. The dynamic recrystallization occurs entirely.

### 3.2.3 Instability factor

The power-dissipation-efficiency diagram is established to clearly distinguish the distribution of power-dissipation efficiency during the thermal deformation. However, the region of material instability cannot be known from this figure. Therefore, Prasad et al. proposed the evaluation criterion of plastic deformation and rheological instability based on Ziegler's criterion of continuous large plastic deformation, and its primary expression is as follows:<sup>14</sup>

$$\xi(\dot{\epsilon}) = \frac{\partial \ln \frac{m}{m+1}}{\partial \ln \dot{\epsilon}} + m < 0 \quad (3)$$

Figure 5 shows the instability diagram of 0N and 0.16N martensitic stainless bearing steel under 0.3, 0.6, and 0.9 strains. The figure shows the relationship between the instability factor and the temperature and strain rate. The yellow region is the unstable region

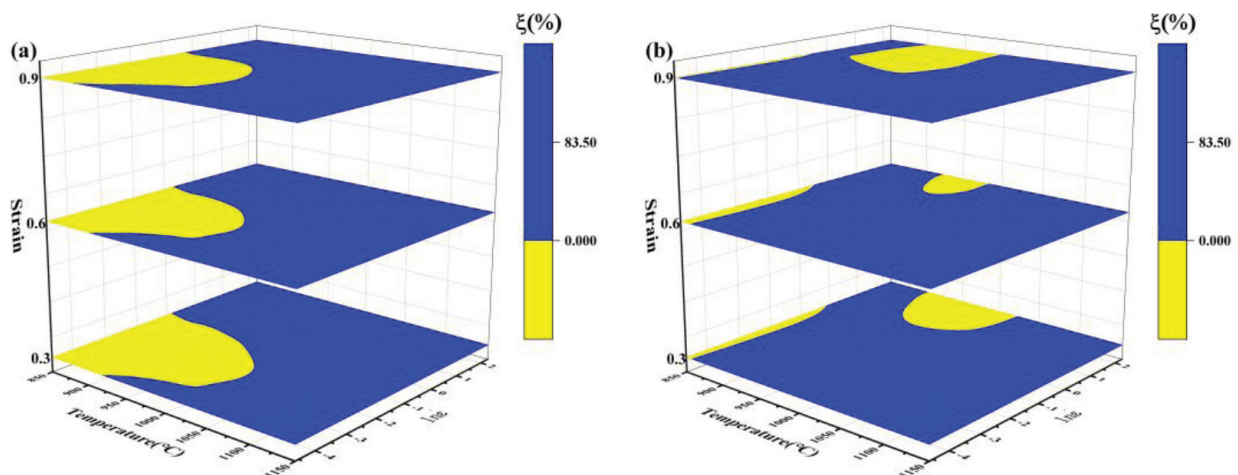


Figure 5: Comparison of instability factors: a) 0.16N bearing steel, b) 0N bearing steel

( $\xi < 0$ ), and the blue region is the stable region ( $\xi \geq 0$ ). The instability zone of 0N bearing steel is mainly concentrated in (875–1000 °C, 0.37–10 s<sup>-1</sup>), and a small part of the instability zone is at low temperature and low strain rate ( $T < 875$  °C, 0.01–1 s<sup>-1</sup>). With the increase of strain, the instability zone decreases and then increases. For 0.16N bearing steel, the instability zone is concentrated at 850–1050 °C, 0.01–0.6 s<sup>-1</sup>, and the instability zone decreases first and then increases with the increase of strain. Generally speaking, the low deformation temperature and high strain rate in thermal working lead to many dislocation proliferation and inter-delivery entanglement, resulting in an unstable flow.<sup>15</sup>

### 3.2.4 Thermal working diagram

Based on the Kumar Prasad criterion, the thermal working diagram of 0.16N and 0N bearing steels can be obtained by superimposing the power-dissipation-efficiency diagram and the instability diagram. The thermal working diagram of the two steels under the conditions of 0.3, 0.6, and 0.9 strains is shown in **Figure 6**.

The optimal processing region should be selected to be as large as possible  $\eta$  under no instability<sup>16</sup>. As shown in **Figures 6a to 6c**, 0.16N, the instability region has little change with the increase of strain, and the essential characteristics of the thermal processing diagram are similar. The instability range under different strains is approximately 850–1025 °C, 0.01–0.6 s<sup>-1</sup>. The thermal working of the 0.16N bearing steel should avoid the low temperature and low strain rate area at 1050–1200 °C,

0.01–0.08 s<sup>-1</sup> suitable for processing. 0N With the increase of strain, the instability region always has two parts, and the essential characteristics of the thermal working diagram are similar. Under different strains, there are instability regions of  $T < 875$  °C, 0.01–1 s<sup>-1</sup>, 875–1000 °C, 0.37–10 s<sup>-1</sup>. The optimal processing region of 0N and 0.16N is also suitable for processing (1050–1200 °C, 0.01–0.08 s<sup>-1</sup>).

### 3.3 Microstructure analysis

Metal plastic deformation is a thermal activation process; at this time the crystal atoms will migrate to a new equilibrium or non-equilibrium position, which requires the atoms' energy to cross a "threshold value," and the energy required is called the deformation activation. The smaller the activation energy, the easier the deformation is to perform. The formula for calculating the activation energy is as follows:<sup>17</sup>

$$Q = R \left[ \frac{\partial \ln(\dot{\epsilon})}{\partial \ln\{\sinh(\alpha\sigma)\}} \right]_T \left[ \frac{\partial \ln\{\sinh(\alpha\sigma)\}}{\partial (1/T)} \right]_{\dot{\epsilon}} \quad (4)$$

The activation energy distributions of 0.16N and 0N under different strains are shown in **Figures 7a and 7b**. For both 0.16N and 0N, Q decreases with the increase of temperature and strain rate under the same strain. With the increase of strain, the area of the high Q value region (red region, 0.16N: greater than 580 kJ/mol; 0N: greater than 510 kJ/mol) shows a decreasing trend. It is not difficult to see that from 0.3 strain to 0.6 strain, the Q value

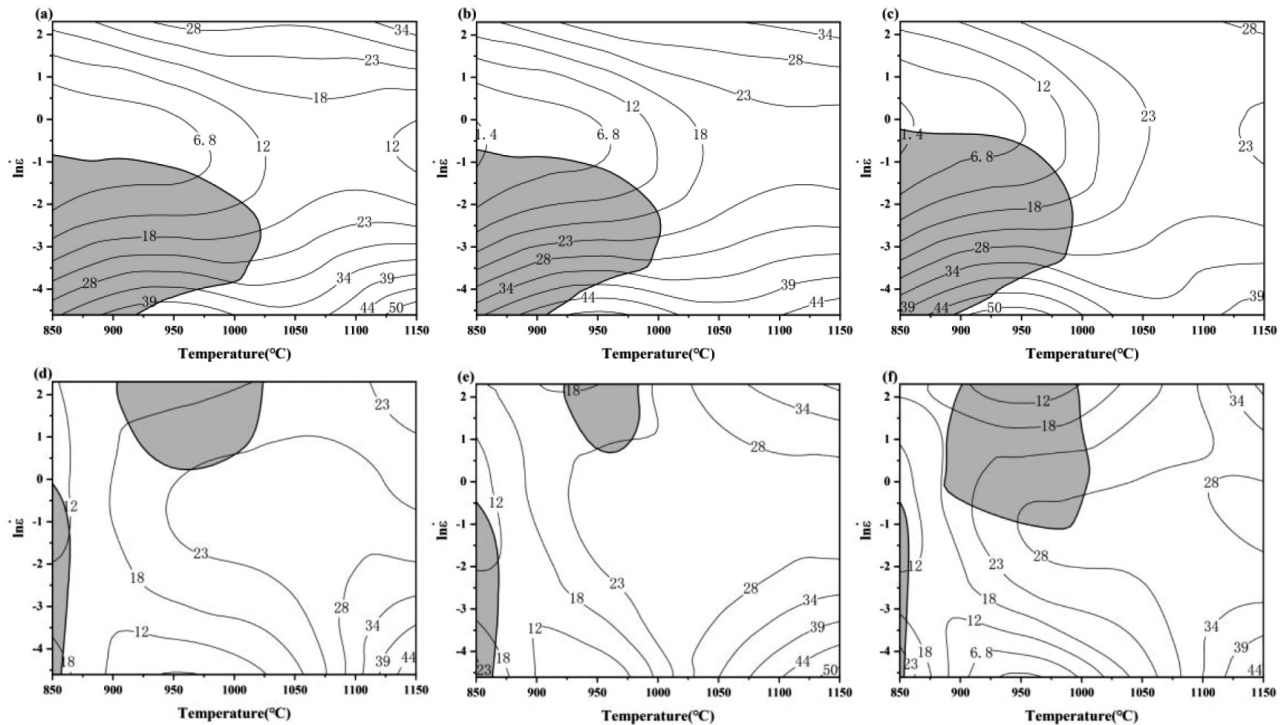


**Figure 6:** Thermal working diagram of 0.16N bearing steel under different strain: a) 0.3, b) 0.6, c) 0.9; Thermal working diagram of 0N bearing steel under different strain: d) 0.3, e) 0.6, f) 0.9

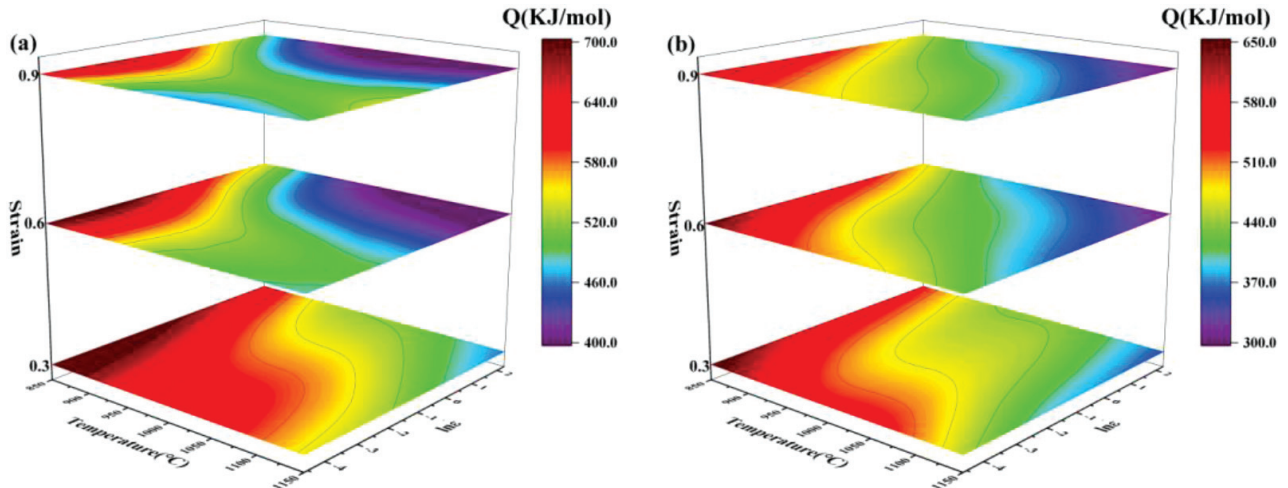


Figure 7: Distribution of deformation activation energy under 0.3, 0.6, and 0.9 strains: a) 0.16N, b) 0N

decreases sharply (taking 0.16N as an example, 587.65 to 511.58 kJ/mol) because the flow stress corresponding to 0.3 strain is close to the peak stress, and the work hardening is the most serious at this time. From 0.6 strain to 0.9 strain,  $Q$  value slowly decreases (taking 0.16N as an example, 511.58 kJ/mol to 494.13 kJ/mol), which is because DRV and DRX phenomena will occur with the increase of strain variable, which can play a softening effect and reduce the degree of work hardening<sup>18</sup>. After 0.6 strain, as shown in **Figure 2b**, the stress-strain curve will enter a relatively smooth phase where deformation is more likely to occur. Compared with the activation-energy-distribution diagram of 0.16N and 0N, the thermal deformation activation energy of 0.16N bearing steel (531.12 kJ/mol(average)) is higher than that of 0N bearing steel (457.99 kJ/mol(average)), indicating that the deformation resistance of 0.16N bearing steel is better than that of 0N bearing steel. This is mainly due to the solid-solution strengthening effect of nitrogen in steel. The existence of nitrogen atoms effectively enhances the deformation resistance of the material.

The temperature distribution and strain rate inside the compressed sample vary greatly, so the region where the temperature and strain rate are consistent with the experimental setting conditions is first determined according to the results. The metallographic diagrams in **Figure 8** were taken after the thermal compression was completed; the strain was 0.916. The diagram of deformation activation energy at 0.9 strain can be analyzed, as shown in **Figure 7a**.  $Q$  decreases with the increase of temperature and strain rate, which is precisely corresponding to **Figure 8**, as shown in **Figure 8b, 8f, 8j** and **8n**. When the strain rate is constant at  $0.1 \text{ s}^{-1}$ , the microstructure at 850 °C is deformed grains caused by the elongation of the original grains, fibrous structures formed at some grain boundaries, and small recrystallized grains. The elongation direction is perpendicular to the compression direction (CD), indicating that dynamic recrystallization

will begin to occur. At 950 °C, the original grains are surrounded by many dynamically recrystallized grains formed near the grain boundaries. The presence of a typical chain structure is formed by bowing out the nucleus at a high-angle boundary (HAB), which is characteristic of discontinuous recrystallization (DDRX) behavior.<sup>19</sup> The results show that grain-boundary expansion induced by strain-induced grain-boundary migration is the primary mechanism of DRX nucleation, and high deformation temperature promotes the DRX process. At 1050 °C there are a large number of small uniform particles. At 1150 °C the recrystallized grains grew uniformly. It shows that the growth of recrystallized grains is the main reason for the microstructure change with increased deformation temperature at high temperatures. In combination with **Figure 7a**, DRX grain growth behavior at 1050–1150 °C is more likely to occur and requires less  $Q$  than DDRX at 850–950 °C.

**Figure 9** compares the microstructure change behavior of 0.16N and 0N at 1050 °C and the upper and lower metallography. Firstly, it can be seen that the recrystallization of 0.16N bearing steel is less than that of 0N bearing steel under the same conditions, but the grains are finer than that of 0N bearing steel. In combination with **Figure 7a** and **7b**, it can be found that  $Q$  of 0.16N is significantly larger than that of 0N, indicating that DRX of 0.16N under the same conditions requires more deformation energy than that of 0N. This is because, with the increase of nitrogen content when the austenite region is experienced in the cooling process of smelting, nitrogen has a more vital refining ability for austenite structure; nitrogen contributes to the short-range ordering of atoms so that it can be pinning dislocation and the interstitial nitrogen atoms have an ability to hinder grain-boundary migration.<sup>20</sup> They can delay grain growth, so the material with a high nitrogen content has finer grains. In addition, by comparing the deformation-activation-energy diagram of 0.16N and 0N (**Figure 7a** and **7b**), at 1050 °C the strain rate of 0N varies from

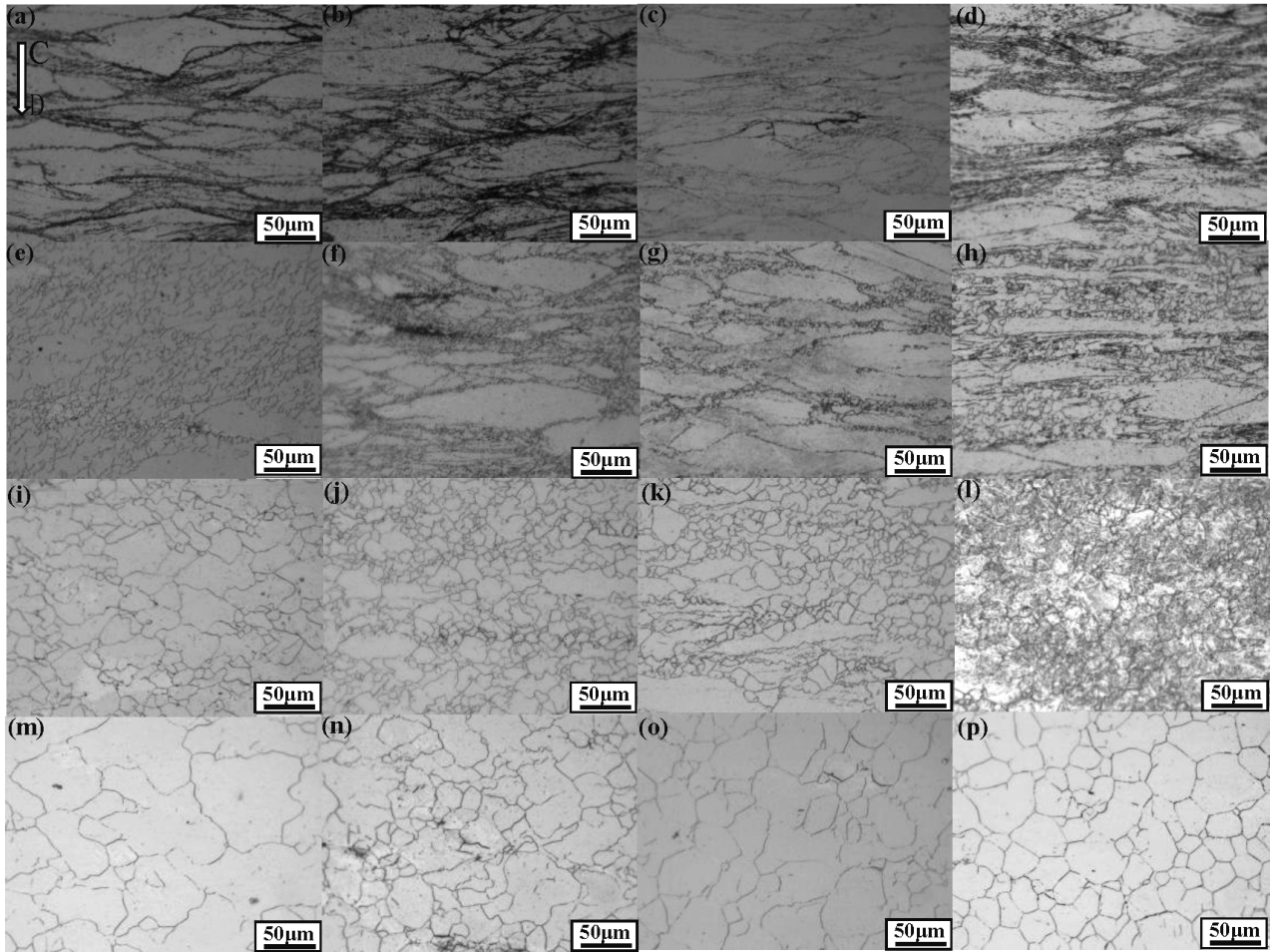


**Figure 8:** metallographic diagram of 0.16N bearing steel: a) 850-0.01 s<sup>-1</sup>, b) 850-0.1 s<sup>-1</sup>, c) 850-1 s<sup>-1</sup>, d) 850-10 s<sup>-1</sup>, e) 950-0.01 s<sup>-1</sup>, f) 950-0.1 s<sup>-1</sup>, g) 950-1 s<sup>-1</sup>, h) 950-10 s<sup>-1</sup>, i) 1050-0.01 s<sup>-1</sup>, j) 1050-0.1 s<sup>-1</sup>, k) 1050-1 s<sup>-1</sup>, l) 1050-10 s<sup>-1</sup>, m) 1150-0.01 s<sup>-1</sup>, n) 1150-0.1 s<sup>-1</sup>, o) 1150-1 s<sup>-1</sup>, p) 1150-10 s<sup>-1</sup>

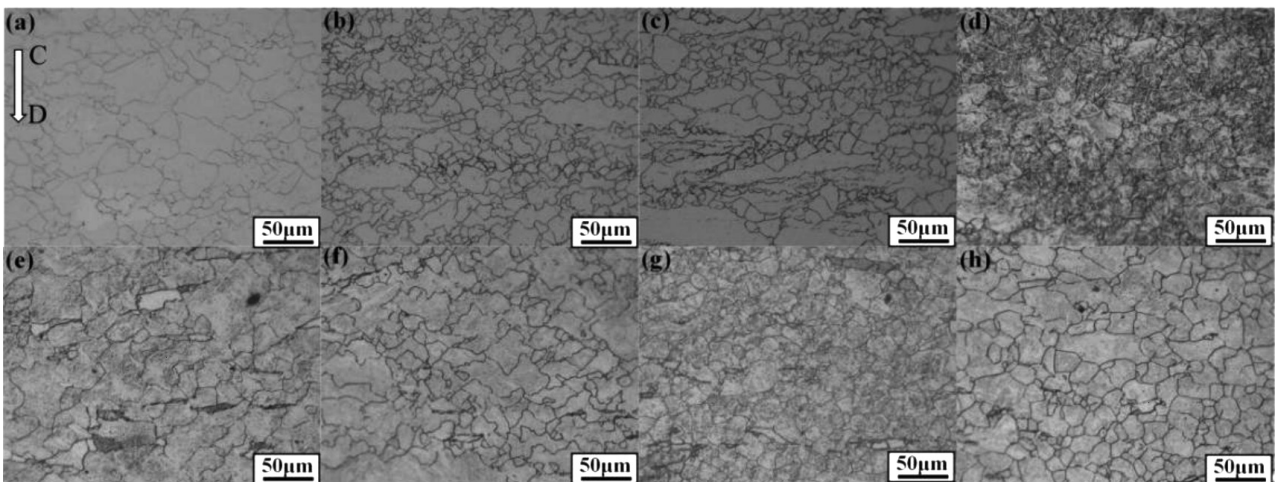


**Figure 9:** Comparison of 0.16N bearing steel and 0N bearing steel metallographic diagram: 0.16N: a) 1050-0.01 s<sup>-1</sup>, b) 1050-0.1 s<sup>-1</sup>, c) 1050-1 s<sup>-1</sup>, d) 1050-10 s<sup>-1</sup>; 0N: e) 1050-0.01 s<sup>-1</sup>, f) 1050-0.1 s<sup>-1</sup>, g) 1050-1 s<sup>-1</sup>, h) 1050-10 s<sup>-1</sup>

0.01–10 s<sup>-1</sup>, and the value of Q does not change much. However, for 0.16N, the color of Q changes from 0.01–0.1 s<sup>-1</sup> (1050 °C), the value of Q changes a little from 0.1–1 s<sup>-1</sup>, and the value of Q also changes significantly from 1 to 10 s<sup>-1</sup>, which is precisely consistent with the change of metallographic diagram. It shows that 0.16 is sensitive to 0.01 s<sup>-1</sup> and 10 s<sup>-1</sup>. Combined with **Figure 9**, at 1050 °C the dynamic recrystallization behavior of 0N has fully occurred, and the strain-rate effect on DRX is less evident than that of 0.16N.

#### 4 CONCLUSIONS

Based on the stress-strain curve, strain-rate-sensitivity diagram, power-dissipation diagram, instability-factor diagram, and thermal working diagram under different strains are constructed. The activation energy of the thermal deformation under different strains was constructed and combined with microstructure analysis.

(1) 0.16N and 0N are both positively sensitive to strain rate and negatively sensitive to temperature. In addition, under the same conditions, the flow stress of 0.16N bearing steel is higher than that of 0N bearing steel, and about 33.724 MPa increases the average peak stress.

(2) The superplasticity of 0N bearing steel usually occurs at high temperature and low speed, while the superplasticity of 0.16N bearing steel tends to shift to low temperature and high speed with the increase of strain. The high  $\eta$  value ( $\eta > 35\%$ ) of 0N bearing steel is mainly concentrated in 1100–1150 °C,  $\dot{\epsilon} < 0.05$  s<sup>-1</sup>, 1125–1150 °C,  $\dot{\epsilon} > 4.5$  s<sup>-1</sup>. The high  $\eta$  value ( $\eta > 35\%$ ) of 0.16N bearing steel is mainly concentrated in 850–1150 °C,  $\dot{\epsilon} < 0.05$  s<sup>-1</sup>. Both 0.16N and 0N are suitable for processing at high temperatures and low rates.

(3) Under the same conditions, the occurrence of DRX in 0.16N bearing steel is less than that in 0N bearing steel, but the grains are finer than those in 0N bearing steel. DRX grain growth at 1050–1150 °C is more likely to occur and requires less Q than DDRX at 850–950 °C, regardless of 0.16 or 0N. At 1050 °C, 0.16 is more sensitive to 0.01 s<sup>-1</sup> and 10 s<sup>-1</sup>, while dynamic recrystallization behavior of 0N has fully occurred, and the effect of strain rate on DRX is not apparent.

#### Acknowledgements

This project is supported by the Central Guiding Local Science and Technology Development Fund Project (YDZJSX2021A036), the Graduate Education Innovation Project of Taiyuan University of Science and Technology (SY2023036), the National Natural Science Foundation of China (52375364), the Basic Research Program of Shanxi Province (TZLH20230818001), and Shanxi Province's Key Core Technology and Common Technology Research and Development Project (20201102017).

#### 5 REFERENCES

- F. Yu, X. P. Chen, H. F. Xu, H. Dong, Y. Q. Weng, W. Q. Cao, Current Status of Metallurgical Quality and Fatigue Performance of Rolling Bearing Steel and Development Direction of High-End Bearing Steel, *Acta Metall. Sin.*, 56 (2020) 4, 513–522, doi:10.11900/0412.1961.2019.00361
- R. Wang, F. H. Li, Z. Q. Yu, Y. Kang, M. Li, Y. Hu, H. R. An, J. Fan, F. Miao, Y. H. Zhao, J. Eckert, Z. J. Yan, Influences of partial substitution of C by N on the microstructure and mechanical properties of 9Cr18Mo martensitic stainless steel, *Mater. Des.*, 236 (2023), doi:10.1016/j.matdes.2023.112497
- M. Seifert, S. Siebert, S. Huth, W. Theisen, H. Berns, New Developments in Martensitic Stainless Steels Containing C plus N, *Steel Res. Int.*, 86 (2015) 12, 1508–1516, doi:10.1002/srin.201400503
- S. J. Zheng, J. H. Liu, L. Xu, S. M. Wen, Z. H. Han, Hot deformation behavior of high nitrogen martensitic stainless steels, *Mater. Res. Express*, 6 (2019) 1, doi:10.1088/2053-1591/aae5e8
- H. Feng, Z. H. Jiang, H. B. Li, W. C. Jiao, X. X. Li, H. C. Zhu, S. C. Zhang, B. B. Zhang, M. H. Cai, Hot Deformation Behavior and Microstructural Evolution of High Nitrogen Martensitic Stainless Steel 30Cr15Mo1N, *Steel Res. Int.*, 88 (2017) 12, doi:10.1002/srin.201700149
- X. Li, L. F. Hou, Y. H. Wei, Z. Y. Wei, Constitutive Equation and Hot Processing Map of a Nitrogen-Bearing Martensitic Stainless Steel, *METALS*, 10 (2020) 11, doi:10.3390/met10111502
- W. J. Liu, J. Li, S. H. Li, J. H. Li, X. J. Li, Effect of Nitrogen on the Hot Deformation Behavior of 0.4C-13Cr Martensitic Stainless Steel, *Steel Res. Int.*, 92 (2021) 8, doi:10.1002/srin.202100020
- Z. G. Nie, G. Wang, J. C. Yu, D. H. Liu, Y. M. Rong, Phase-based constitutive modeling and experimental study for dynamic mechanical behavior of martensitic stainless steel under high strain rate in a thermal cycle, *Mech. Mater.*, 101 (2016), 160–169, doi:10.1016/j.mechmat.2016.08.003
- J. Y. Zhang, Y. Tang, H. M. Zhou, Q. Chen, J. Zhou, Y. Meng, Investigation on thermal rheological behavior and processing map of 30CrMnSiNi2A ultra-strength steel, *Int. J. Mater. Form.*, 14 (2021) 4, 507–521, doi:10.1007/s12289-019-01531-1
- W. Feng, F. Qin, H. Long, Hot workability analysis and processing parameters optimisation for 20CrMnTiH steel by combining processing map with microstructure, *IRONMAKING & STEELMAKING*, 45 (2018) 4, 317–324, doi:10.1080/03019233.2016.1264145
- H. A. Lin, M. S. Yang, B. Song, Study on hot compressive deformation behavior and microstructure evolution of G13Cr4Mo4Ni4V steel, *Mater. Today Commun.*, 38 (2024), doi:10.1016/j.mtcomm.2024.108429
- Y. C. Zhu, Q. H. Wang, Z. Q. Huang, L. Qin, Z. L. Li, L. F. Ma, Strain Hardening Exponent and Strain Rate Sensitivity Exponent of Cast AZ31B Magnesium Alloy, *METALS*, 12 (2022) 11, doi:10.3390/met12111942
- L. Chen, B. Zhang, Y. Yang, T. L. Zhao, Y. Xu, Q. Wang, B. Zan, J. Cai, K. S. Wang, X. Chen, Evolution of hot processing map and microstructure of as-forged nickel-based superalloy during hot deformation, *J. Mater. Res. Technol.*, 24 (2023), 7638–7653, doi:10.1016/j.jmrt.2023.05.060
- J. Luo, M. Q. Li, Efficiency of Power Dissipation and Instability Criterion for Processing Maps in Hot Forming, *CMC-Comput. Mater. Continua*, 18 (2010) 3, 271–299
- L. Han, H. Y. Zhang, J. Cheng, G. Zhou, C. Wang, L. J. Chen, Thermal Deformation Behavior of Ti-6Mo-5V-3Al-2Fe Alloy, *CRYSTALS*, 11 (2021) 10, doi:10.3390/cryst11101245
- H. Y. Qin, Z. T. Li, G. P. Zhao, W. Y. Zhang, Q. Tian, C. Wang, Hot Deformation Behavior and Microstructure and Mechanical Properties Evolution of Forged GH4742 Superalloy, *Rare Met. Mater. Eng.*, 51 (2022) 11, 4227–4236

- <sup>17</sup> Y. H. Song, Z. H. Cai, G. H. Zhao, Y. G. Li, H. Y. Li, M. X. Zhang, Hot deformation behavior of 309L stainless steel, *Mater. Today Commun.*, 36 (2023), doi:10.1016/j.mtcomm.2023.106877
- <sup>18</sup> L. X. Li, B. Ye, S. Liu, S. D. Hu, B. Li, Inverse analysis of the stress-strain curve to determine the materials models of work hardening and dynamic recovery, *Mater. Sci. Eng., A*, 636 (2015), 243–248, doi:10.1016/j.msea.2015.03.115
- <sup>19</sup> L. X. Ouyang, R. Luo, Y. W. Gui, Y. Cao, L. L. Chen, Y. J. Cui, H. K. Bian, K. Aoyagi, K. Yamanaka, A. Chiba, Hot deformation characteristics and dynamic recrystallization mechanisms of a Co-Ni-based superalloy, *Mater. Sci. Eng., A*, 788 (2020), doi:10.1016/j.msea.2020.139638
- <sup>20</sup> T. Masumura, T. Tsuchiyama, S. Takaki, T. Koyano, K. Adachi, Difference between carbon and nitrogen in thermal stability of metastable 18 %Cr-8 %Ni austenite, *Scr. Mater.*, 154 (2018), 8–11, doi:10.1016/j.scriptamat.2018.05.019